Influence of the tribological properties of the Zr,Hf-(Zr,Hf)N-(Zr,Me,Hf,Al)N coatings (where Me is Mo, Ti, or Cr) with a nanostructured wear-resistant layer on their wear pattern during turning of steel

Sergey Grigoriev [a], Alexey Vereschaka [b,*], Vladimir Uglov [c], Filipp Milovich [d], Vladimir Tabakov [e], Nikolai Cherenda [c], Nikolay Andreev [d], Mars Migranov [a]

[a] Moscow State Technological University STANKIN, Vadkovsky per. 1, Moscow, 127994, Russia
[b] IDTI RAS, Vadkovsky per. 18-1a, Moscow, 127994, Russia
[c] Belarusian State University, Physics Faculty, Nezavisimosti Ave. 4, 220030, Minsk, Belarus
[d] National University of Science and Technology "MISiS", Leninsky Prospect 4, Moscow, 119049, Russia
[e] Ulyanovsk State Technical University, SevernyiVenec 32, 432027, Ulyanovsk, Russia

ARTICLE INFO

Keywords:
Tribological properties
Nanostructured coatings
Turning of steel
Tool wear
Oxidation

ABSTRACT

An increase in the speed of cutting and, accordingly, the temperature in the zone of cutting predetermines the need to develop wear-resistant coatings, functioning effectively under such operation conditions. One of the key functions of the coating is the creation of optimal tribological conditions under the influence of temperatures and force factors of the operation of the coating. The coatings of Zr,Hf-(Zr,Hf)N-(Zr,Me,Hf,Al)N (Me is Mo, Ti, or Cr) with nanostructured wear-resistant layer were studied. At temperatures up to 700 °C, the minimum adhesive component f_{adh} of the friction coefficient was exhibited by a coating containing chromium (Cr), and at temperatures above 700 °C – by a coating containing molybdenum (Mo). At the turning of steel, the highest resistance to wear at the speed of cutting of v_c = 250 m/min was exhibited by a tool with a Cr-containing coating, and at the speed of cutting of v_c = 400 m/min – by a tool with a Mo-containing coating. Thus, the optimal composition of the coating depends on the speed of cutting. Information about the adhesive component f_{adh} of the coefficient of friction makes it possible to fairly reliably predict the wear rate of the tool during cutting under the conditions of the temperatures corresponding to the temperatures at which the value of f_{adh} was measured.

It has been found that an oxide layer with a complex structure is formed in the areas of the coatings adjacent to a wear crater. Iron (Fe) and its oxide dominate in the outer regions of this oxide layer, a high content of aluminum (Al) oxide is detected in the intermediate region, and oxides of zirconium (Zr), titanium (Ti), chromium (Cr), and hafnium (Hf) dominate in the inner region.

1. Introduction

Modern coatings are expected not only to have high hardness and wear resistance, but they should also provide resistance to brittle fracture, elevated temperatures, and associated processes of diffusion and oxidation [1–3]. The intensification of cutting modes, in particular, an increase in cutting speed [4–6] when using cutting tools with wear-resistant coatings, contributes to the need for the further improvement of their physical-mechanical properties. The improvement of the wear-resistant coatings goes in two main directions:

- Complication of a coating structure due to the creation of coatings with a different number of functional layers and with a nanolayered structure [7–9];
- Complication of the ratio of elemental content in the coatings through the introduction of additional metals and non-metals, the use of not only nitride, but also oxide, carbonitride, and oxynitride coatings [10–13].

The (Ti,Al)N-, (Zr,Al)N-, and (Cr,Al)N-based coatings are widely used which is explained by their high performance properties [14–16]. Aluminum (Al) introduces into the composition of TiN, ZrN, and CrN

Table 1
Density and molar mass of the oxide and nitride phases of hafnium and zirconium.

	Density, g/cm³ [29]	Molar mass, g/mol [29]	Poisson's ratio	Gibbs energy (25°C), kJ/mol
HfN	11.70	192.50	0.14 [30]	4.68 [31]
HfO_2	9.68	210.19	0.32 [32]	—1010 [33]
ZrN	7.09	105.23	0.16 [30]	6.96 [31]
ZrO_2	5.68	123.22	0.27 [32]	—1100 [33]

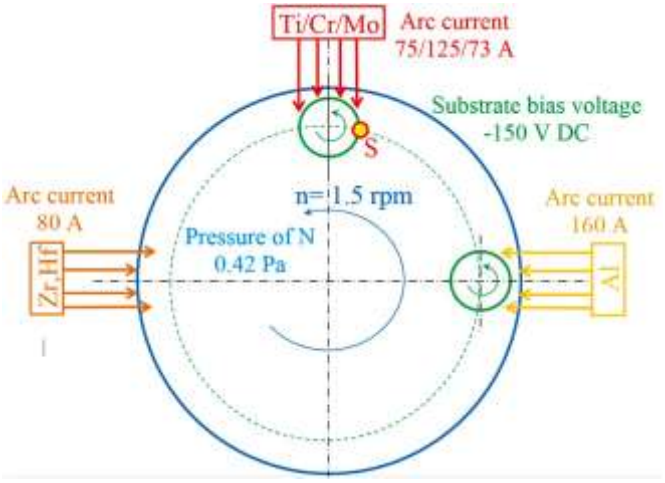

Fig. 1. A schematic diagram of sample S movement during coating deposition in the VIT-2 unit.

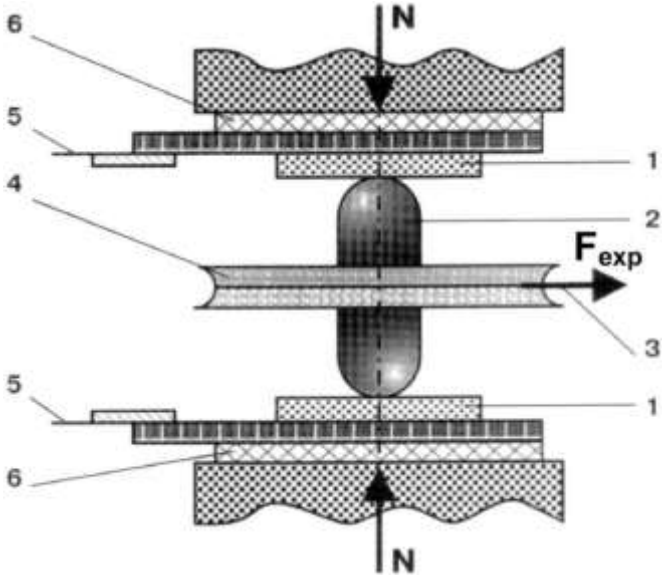

Fig. 2. Model of friction contact [60,71–73].

increases the hardness and heat resistance of these systems due to the effect of crystal lattice distortion [17,18], and furthermore, a certain positive effect is provided by an oxide film of Al_2O_3 formed on the surface of such coatings [19,20]. A further increase in the properties of these coatings can be obtained due to the additional elements introduced into their composition, including hafnium (Hf) and molybdenum (Mo). The conducted studies find that the introduction of Hf and Mo into the composition of the coating not just increases the hardness and wear resistance of the coatings, but also improves their heat resistance and

Table 2
Outcome of the study of the coating composition.

Coating	Element content, at. %					
	Zr	Hf	Al	Cr	Ti	Mo
H1	41.9 ± 8.1	19.2 ± 2.3	9.4 ± 3.2	–	–	29.5 ± 7.2
H2	43.0 ± 7.3	19.7 ± 3.1	11.3 ± 3.6	–	26.0 ± 7.7	–
H3	42.3 ± 8.8	18.1 ± 3.3	10.1 ± 4.1	29.5 ± 8.3	–	–

tribological properties [21–23]. At the elevated temperatures which are typical for the cutting zone, oxide films of MoO_2 and HfO_2 are formed in the surface layers of the Mo- and Hf-containing coatings. These oxide films both perform protective functions against further oxidation and positively transform contact processes in the cutting zone [24,25]. The presence of Zr in the composition of the coating enhances resistance to cracking and to brittle fracture [26,27]. Along with these oxides, films of ZrO_2 can also improve the tribological parameters of the cutting process [28].

This paper considers the (Zr,Hf,Al)N-based multilayer coatings, with such elements as Cr, Ti, or Mo additionally introduced in the wear-resistant layer of the coatings. Due to the close ionic radii of Hf (0.83 Å for coordinate number 8) and Zr (0.84 Å for coordinate number 8), when nitride phases with the same unit cell are formed, the lattice parameters of these compounds will also be fairly close. But with almost identical lattice parameters, the density of phases with Hf will be significantly (almost two times) higher due to the larger mass of the Hf element. The same is valid for the oxide phases of HfO_2 and ZrO_2 (see Table 1).

An analysis of the change in Poisson's ratio (see Table 1) shows that nitrides are noticeably more brittle than oxides, with HfO_2 being the most ductile of the considered compounds. Hafnium and zirconium oxides differ significantly in mass, and, therefore, in density, which is clearly seen from Table 1.

The density of hafnium oxide is almost twice that of zirconium oxide, which affects hardness and other physical and chemical parameters. It is also known that hafnium is a more inert metal relative to zirconium, as evidenced by the difference in Gibbs energies at room temperature for HfO_2 and ZrO_2. The lower Gibbs energy of ZrO_2 relative to HfO_2 makes it more likely that zirconium oxide is formed from the decomposition of zirconium nitride than that of hafnium oxide from the decomposition of hafnium nitride. As the temperature rises during cutting, the difference in Gibbs energies becomes more significant [34].

At the same time, the mechanical, electrophysical, and thermal-conductive properties of the nitride and oxide phases of Hf and Zr differ significantly. A slight substitution (up to ~ 6 at%) of zirconium cations in the nitride phase of ZrN and the fluorite phase of ZrO_2 is unlikely to significantly affect the mechanical properties of these compounds; however, several authors note certain advantages of the coating of (Zr,Hf)N in comparison with the coating of ZrN [35,36]. The properties of the system of (Zr,Hf)N will be considered in more detail. The ZrN coatings are well known and widely used [37,38]. Hafnium (Hf) introduced into the ZrN composition contributes to the formation of the dominant c-(Zr,Hf)N phase, which has certain advantages compared to the c-ZrN phase. Several studies note that the (Zr,Hf)N coating has a slightly higher hardness compared to the ZrN coating [35,36]. Increased adhesion to the carbide alloy is typical for Hf-containing coatings [39,40]. The (Zr,Hf)N coating has a dense columnar structure [41,42]. Another effect of introduced Hf is a slight decrease of internal stresses [43,44]. The significant effect of introduced Hf is related to an increase in the resistance of the coating to oxidation [36]. The better resistance to oxidation may be related to a decrease in oxygen diffusion, a growth in stoichiometry, and elevated thermal stability of the HfN system [45]. In this case, very high Hf content in the coating can, on the contrary,

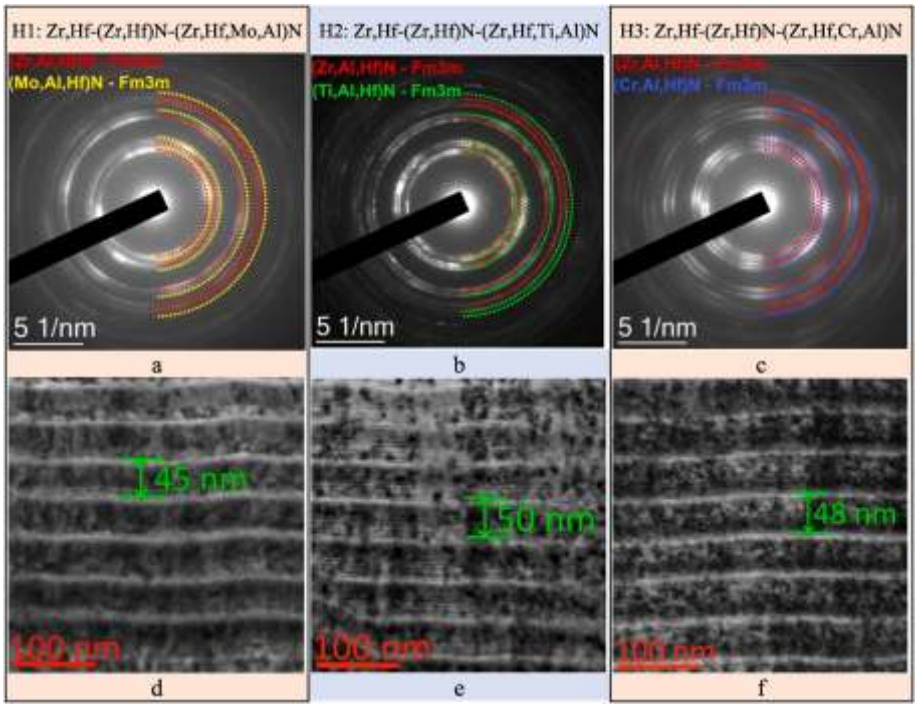

Fig. 3. (a–c) Results of the selected area electron diffraction pattern (SAED) analysis and (d–f) parameters of the coating nanostructure.

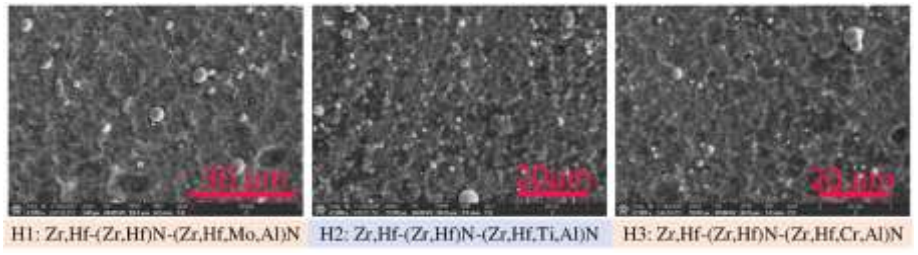

Fig. 4. Morphology of the surface of the samples coated with the coatings under consideration.

worsen the resistance to oxidation [36,45].

The introduction of hafnium can also improve the properties of the (Ti,Al)N coating. In particular, a growth of hardness, wear resistance [46], and heat resistance [47] is observed. The elevated heat resistance is related to the higher temperature at which the active formation of h-AlN and spinodal decomposition begin [47]. Due to this effect, the (Ti, Al,Hf)N coating retains its high hardness at temperatures up to 900 °C [48]. Hafnium (Hf) introduced into the coating of (Ti,Al)N also contributes to the effect of a considerable increase in the resistance to oxidation at high temperatures, due to the slowdown in the transformation of metastable TiO_2 (anatase) into stable TiO_2 (rutile) [47]. The oxidation process in the coating of (Ti,Al,Hf)N, in contrast to the coating of (Ti,Al)N, results in the forming oxide films with nanolayered structure (with nanolayers, rich in Al or Ti). The films with such structure better protect the coating from further oxidation [49].

Hafnium introduced into the (Ti,Cr)N system also contributes to a considerable increase in the wear resistance of the coating [50] and provides favorable combination of high hardness and a low elastic modulus [51]. The coating of (Hf,Mo)N also exhibits good properties. When the coating is heated to the temperature of 600 °C, the formation of a dense outer oxide layer is detected, which not only protects it against further oxidation, but also reduces the friction coefficient [52].

An additional increase in the resistance to wear and heat is provided by the multicomponent coatings that combine nitrides of Ti, Hf, Zr and some other metals [53–57]. In particular, these coatings exhibited the formation of surface oxide films with the positive properties described earlier.

Beside the optimized elemental composition, an improvement in the coating properties can be achieved due to a complex multilayer architecture that provides for the presence of several functional layers with an outer wear-resistant layer of a nanolayered structure [58–60]. The conducted studies find that the application of a coating architecture with three functional layers (adhesive, transition, and wear-resistant layers) has certain advantages in comparison with single-layer coatings [59, 60]. The rational choice of the modulation period λ of the wear-resistant layer can provide further improvement of the coating properties [61].

This paper considered three coatings as follows:

- Zr,Hf-(Zr,Hf)N-(Zr,Hf,Mo,Al)N, designated as Coating H1;
- Zr,Hf-(Zr,Hf)N-(Zr,Hf,Ti,Al)N, designated as Coating H2; and
- Zr,Hf-(Zr,Hf)N-(Zr,Hf,Cr,Al)N, designated as Coating H3.

2. Materials and methods

For all three coatings, an identical architecture was chosen, consisting of an adhesive layer 20–50 nm thick (based on Zr–Hf), a transition layer 0.7–1.0 μm thick (based on (Zr,Hf)N), and a wear-resistant layer about 3 μm thick (based on (Zr, Hf,Me,Al)N (Me was Mo, Ti, or Cr) [59,60]. The nitride layers of the coatings contained about 50 at% nitrogen. The wear-resistant layer of all coatings had a nanolayered

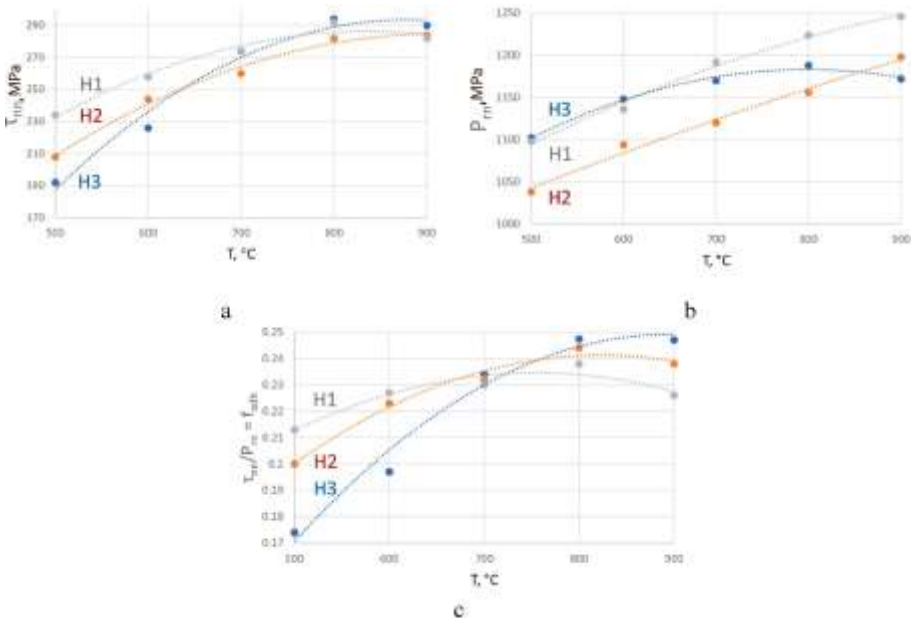

Fig. 5. Outcome of the studies of the tribological properties of the coatings: (a) shear strength of the adhesive bonds τ_{nn}, (b) normal stresses acting on the surface of the indented p_n, (c) adhesion (molecular) component f_{adh} of the friction coefficient.

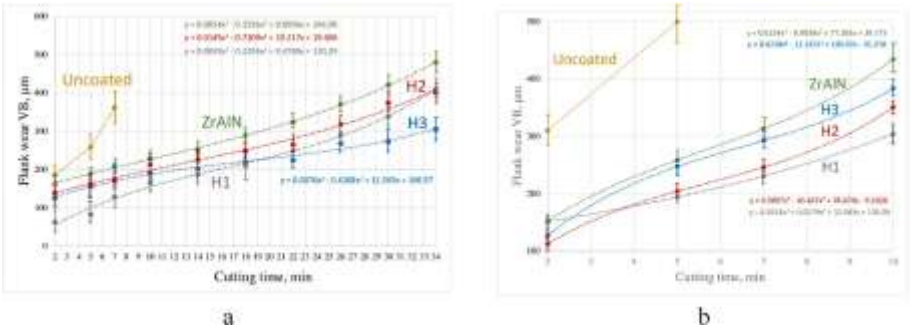

Fig. 6. Results of the study of flank wear rate on the samples. (a) v_c = 250 m/min, (b) v_c = 400 m/min.

structure with the nanolayer period λ of about 50 nm [62].

The process of coating deposition was carried out using a special VIT-2 unit (IDTI RAS – MSTU STANKIN, Russia) [63–68], which implemented the filtered cathodic vacuum arc deposition (FCVAD) technology [63] and the Controlled Accelerated Arc (CAA-PVD) [69]. To deposit the coatings, the cathodes were used as follows: cathode of Al (99.8%) was installed on the FCVAD system evaporator, and cathodes of Zr, Hf (65.5 + 34.5%), as well as, depending on the coating type, cathodes of Cr (99.8%), Mo (99.7%), or Ti (99.9%) were installed on the CAA-PVD system evaporators. A schematic diagram of sample S movement during coating deposition in the VIT-2 unit is shown in Fig. 1.

The formation of nanolayered structure of the wear-resistant coating layer took place at planetary rotation (controlled) of the samples in chamber, with the combination of plasma flows from the FCVAD and CAA-PVD evaporators, at the rotation speed of a turntable of n = 1.5 rpm. The coatings were deposited onto carbide inserts of SNUNISO (WC+15% TiC+6% Co) (of commercial purpose). Before the deposition of the coatings, the samples underwent the following preparation procedure: washing by the solution of chemically active substances, with ultrasonic stimulation, washing by purified running water, and drying by a stream of hot purified air. After the placement of the samples in the chamber, air had been pumped out and an inert gas (argon) had been supplied, the samples underwent ion cleaning and thermal activation in a flow of a gas (argon) and metallic (Zr, Hf) plasma. The process of coating deposition took place at the parameters: arc current was 160 A for the aluminum cathode, 80 A – for the Zr–Hf cathode, 75 A – for the titanium cathode, 125 A – for the molybdenum cathode, and 73 A – for the chromium cathode. A pressure of nitrogen of 0.42 Pa was maintained during the process of coating deposition. The substrate bias voltage was —150 V DC for all three coatings.

An automated mechanical tester SV-500 (Nanovea, USA) with a nanomodule was used to measure hardness and modulus of elasticity. Instrumental indentation with a Berkovich indenter was carried out at a load of 50 mN.

The measurements of the adhesive bond strength with the substrate were conducted in accordance with ASTM C1624-05 [70].

A Carl Zeiss EVO 50 scanning electron microscope (SEM) equipped with an energy-dispersive X-ray spectroscopy (EDX) system X-Max - 80 mm2 (OXFORD Instruments) was used. The survey was carried out with backscattered electrons (20 kV, 750 pA).

A JEM 2100 (JEOL, Japan) transmission electron microscope (TEM) at the accelerating voltage of 200 kV was applied to study the micro- and nanostructures. The coating composition was considered with the TEM with an INCA Energy EDX system (OXFORD Instruments). Samples (lamellas) for research were cut out with a focused ion beam (FIB) Strata 205 (FEI, USA).

Tribological properties were determined using a special adhesive meter [60,71–73]. Fig. 2 shows a diagram of this adhesion meter, which

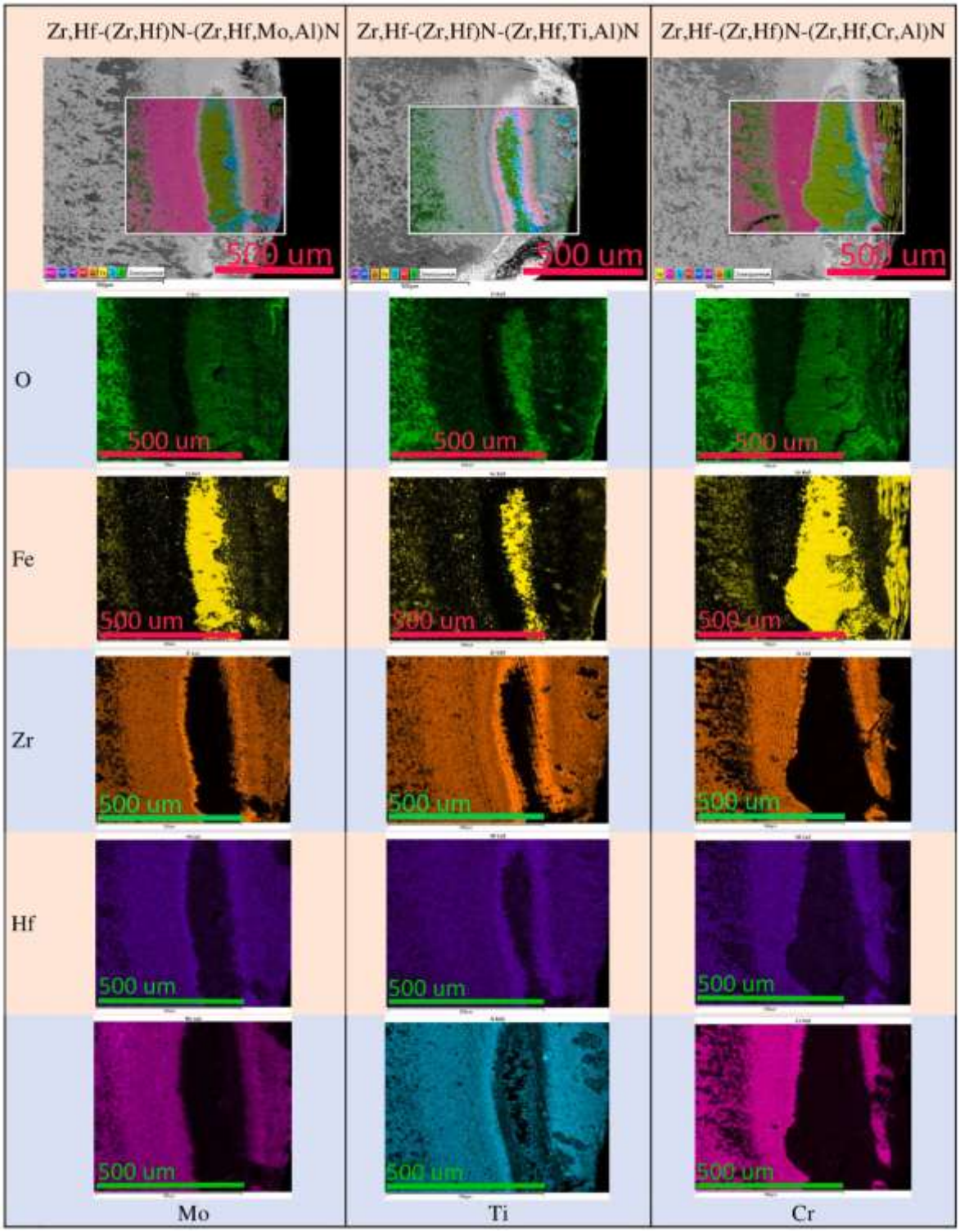

Fig. 7. Mapping the content of elements in the crater area on the rake face of the samples with the studied coatings (v_c = 400 m/min).

includes a carbide indenter 2 with a spherical tip, which simulates a cutting tool in contact with the cut material during turning. A coating is deposited on this indenter. This indenter is compressed by two parallel plates 1, which are made of AISI 321 steel.

A force N is applied to the plates, due to which they compress the indenter. The steel cable 3 in the groove of the disk 4 is subjected to the force F_{exp} necessary for the rotation of the indenter 2. This force is mainly related to the shear strength τ_n of the adhesive shear bond, which is determined by the formula:

$$\tau_{nn} = \frac{3}{4} \cdot \frac{F_{exp}}{\pi} \cdot \frac{R_{exp}}{r_{ind}^3} \quad (1)$$

where F_{exp} is the force, applied to the disk rotating the indenter;

R_{exp} is the radius of the disk with the installed indenter;

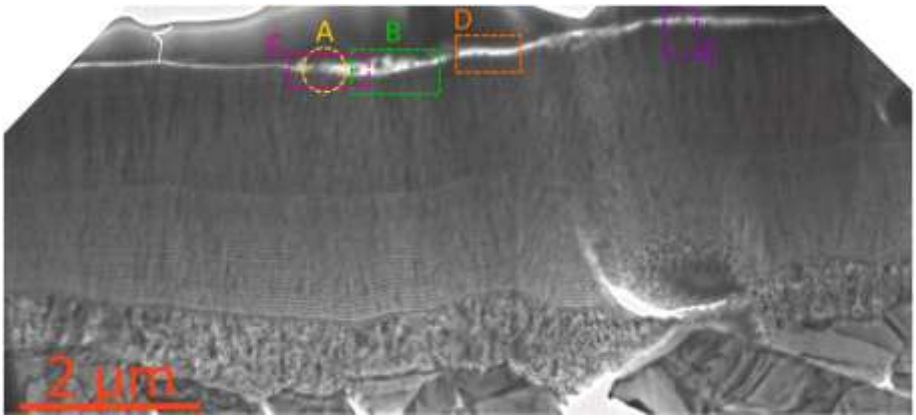

Fig. 8. Overall view of the lamella with indication of the location of Areas A-E under consideration.

r_{ind} is the radius of an indentation formed by the indenter tip on the plates 1.

Due to the small size of the imprint, it is assumed that the normal stresses P_{rn} acting on the surface of the sphere are constant and the same over the entire area of the imprint. These stresses are determined by the formula:

$$P_{rn} = \frac{N}{n \cdot r_{ind}^2} \quad (2)$$

Thus, the adhesion (molecular) component of the coefficient of friction (COF) can be found from the formula as follows:

$$f_M = \frac{\tau_{nn}}{p_{rn}} = \frac{3}{4} \cdot \frac{F_{exp}}{N} \cdot \frac{R_{exp}}{r_{ind}} \quad (3)$$

To simulate the effect of temperatures in the cutting zone, the equipment used uses induction heating of plates 1 by electric current supplied through conductors 5. Heat-insulating pads 6 are necessary to isolate the heating zone.

The turning of steel 1045 with plates with the coating under study was carried out on a CU 500 MRD lathe (Sliven) with a ZMM CU 500 MRD variable-speed drive under dry cutting conditions at cutting modes: feed (f) = 0.1 rpm, depth of cut (a_p) = 0.5 mm, cutting speed (v_c) = 250 and 400 m/min [74,75]. The objects of comparison were uncoated plates and plates with the commercial ZrN coating. Five cutting tests were conducted for each type of coating.

3. Results

3.1. Study of elemental ratio and phase composition and structure of coatings

Given that the elemental composition changes within the coating thickness depending on nanolayered structure and the presence of nanolayers with a predominance of certain elements, the coating composition was measured along a line 200 nm long, with an interval of 10 nm. Table 2 contains the average data and the deviations detected during the measurement.

It has been found that each of the studied coatings consists of two fcc phases of cubic solid solutions: (Zr,Al,Hf)N and (Mo,Al,Hf)N; (Zr,Al,Hf)N and (Ti,Al,Hf)N; (Zr,Al,Hf)N and (Cr,Al,Hf)N for Coatings H1, H2, and H3, respectively, (Fig. 3 a-c). Due to the intensity of the rings in the electron diffraction pattern in Coatings H2 and H3, it can be assumed that the amount of both phases in the structure was approximately the same, and a slight difference in the content was noticeable only in Coating H1, where the content of the (Zr,Al,Hf)N phase slightly prevailed over the (Mo,Al,Hf)N phase.

All three coatings have a well-defined nanolayered structure, and the value of the modulation period λ is 45, 50 and 48 nm, respectively, for Coatings H1, H2, and H3 (Fig. 3 d-f).

The surface morphology of the coatings is generally identical (Fig. 4). There is a cluster structure with a typical cluster size of 3–5 μm. A moderate amount of microparticles, identical for all three coatings, is detected on the coating surface.

3.2. Study of mechanical and tribological properties of coatings

According to the conducted studies, the considered coatings have fairly close hardness. The highest hardness (28.70 ± 0.80 GPa) was exhibited by Coating H2, which may be associated with the high hardness of the (Ti,Al)N phase [76]. The lowest hardness is typical for Coating H3 (26.30 ± 0.70 GPa), and the hardness of Coating H1 is 27.20 ± 0.40 GPa. The hardness of the ZrN (reference) coating was 25.10 ± 1.10 GPa.

During the scratch test, the critical fracture load L_{C2} reached 32, 34, and 35 N for Coatings H1-H3, respectively, and 35 N for the ZrN (reference) coating.

Following the study of the tribological properties of Coatings H1-H3 (Fig. 5), it is found that these parameters change significantly with increasing temperature. At the temperature of 500 °C, Coating H3 has the best tribological properties (in particular, the smallest adhesive component f_{adh} of friction coefficient, and as the temperature rises to 700 °C, all three coatings have close values of f_{adh}. As the temperature increases further to 900 °C, Coating H1 exhibits a noticeable decrease in the value of f_{adh}, which indicates the best tribological properties of Coating H1 under these conditions. Taking into account that the temperature in the zone of cutting changes depending on the speed of cutting [77], it can be assumed that when being operated at high cutting speeds and, accordingly, high temperatures, Coating H1 will have the best tribological properties, while Coating H3 will have the best tribological properties at lower cutting speeds and, respectively, at lower temperatures.

3.3. Study of wear resistance of coated cutting tools at different cutting speeds

The investigation of the resistance to wear of the coated tools was carried out in turning of steel 45 at two speeds of cutting, 250 and 400 m/min. It has been found that at the speed of cutting of 250 m/min, the tool with Coating H3 has the best wear resistance (Fig. 6 a). It should be noted that the obvious advantage in the resistance to wear of the tool with Coating H3 begins to be noticeable after 18 min of cutting. Up to 18th minute of cutting, Coating H1 exhibits the best resistance to wear, but after 18 min of cutting, the wear rate increases markedly.

As the speed of cutting increases up to 400 m/min, the wear rate of

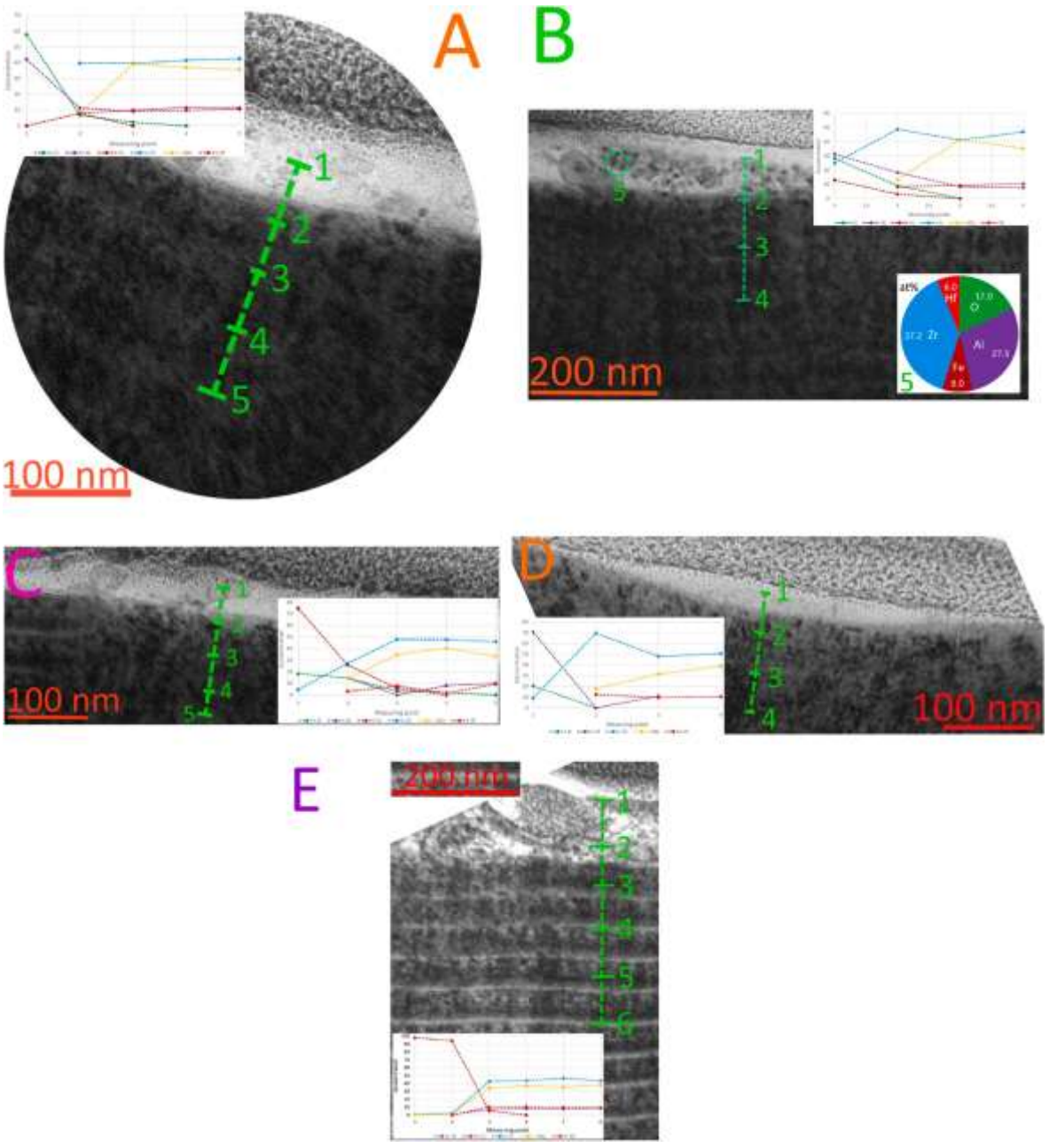

Fig. 9. Results of the studies of the processes of oxidation on the coating surface in the area of elastic contact with the flow of the machined material (Areas A-E).

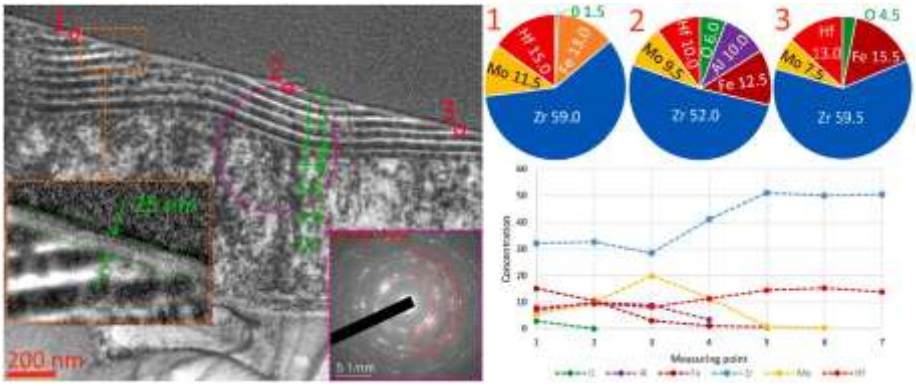

Fig. 10. Outcome of the studies of the oxidation and diffusion processes on the worn surface of the coating.

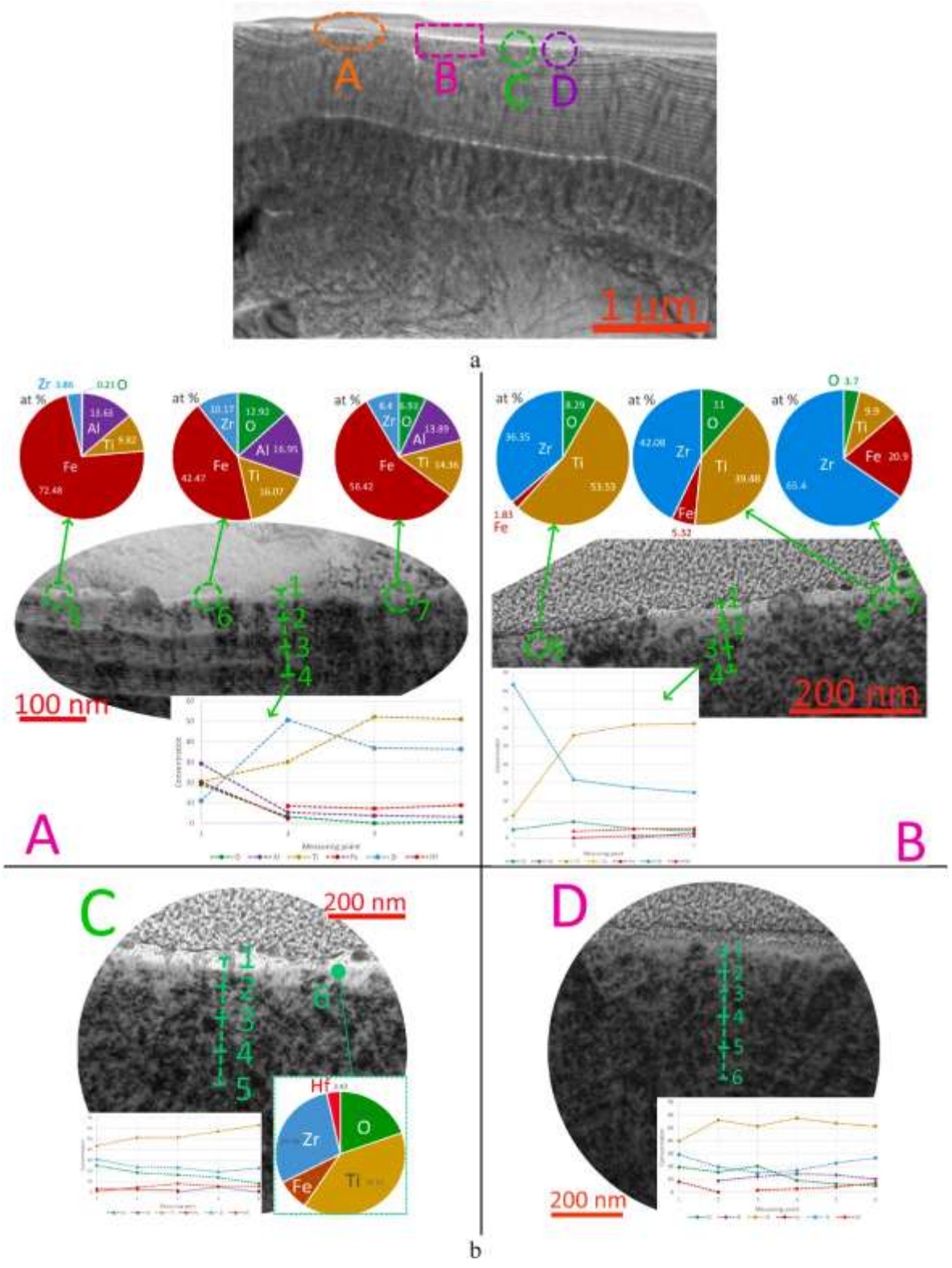

Fig. 11. (a) Area of Coating H2 under study, located as close as possible to the wear crater boundary, (b) outcome of the analysis focused on the elemental composition of the studied area.

the tool increases markedly, and it varies more significantly for different coatings. The highest wear resistance at the given cutting speed was exhibited by the tool with Coating H1. Since as high cutting speeds result in a noticeable increase in temperature in the zone of cutting, the role of adhesive-fatigue factors decreases, and the role of the oxidation and diffusion processes increases [78,79], it can be assumed that Coating H1 has the best resistance to these wear mechanisms among the coatings under study.

An important trend in the intensification of machining is the increasing of a cutting speed [80]. Taking this into consideration, the features of tool wear with coatings at the speed of cutting of 400 m/min were studied in more detail.

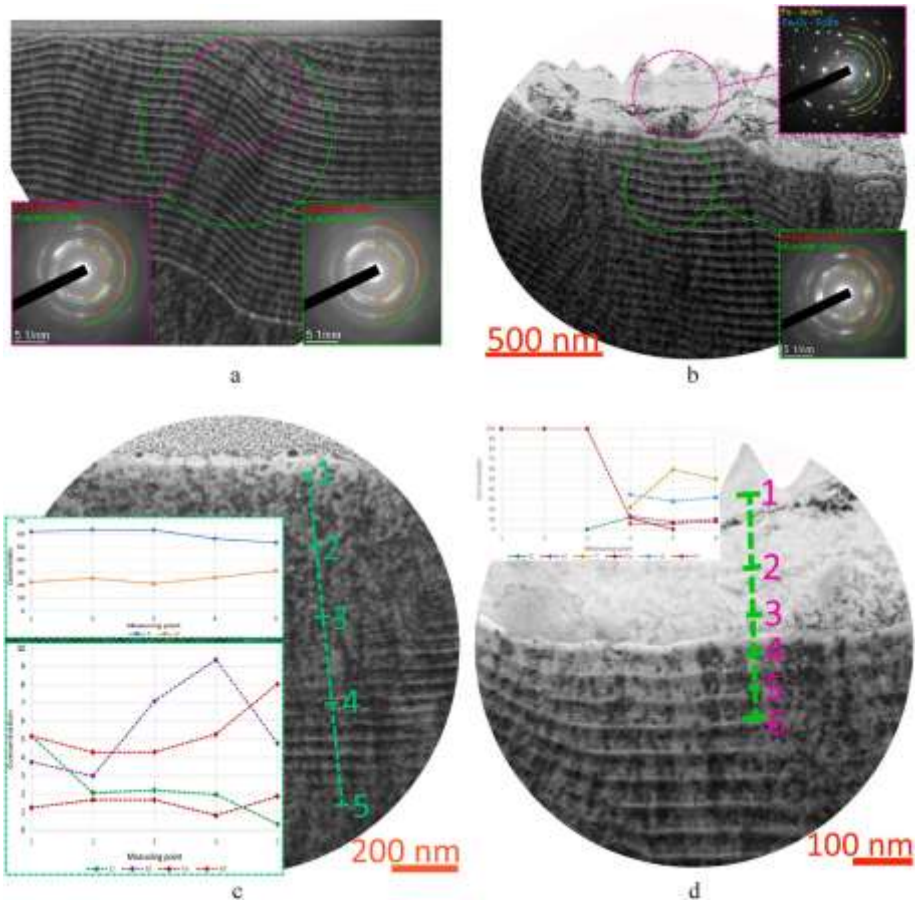

Fig. 12. (a) Adherent-free area of the worn coating, (b) outcome of the study of the processes of oxidation and diffusion in the area, (c) area of dense plastic contact, (d) outcome of the study of the processes of oxidation and diffusion in this area.

As can be seen in Fig. 7, the studied coatings have a fairly similar wear pattern (in particular, the formation of a wear crater on the front surface is observed). The differences are related only to the intensity of wear of the H3 coating. Since the coatings have fairly similar hardness (and, accordingly, resistance to abrasive wear), shear strength of the adhesive bonds (and, accordingly, resistance to adhesive fatigue wear), the difference in wear intensity can be due to oxidative and diffusion processes. Fig. 7 depicts maps of the elemental distribution in the coating on the rake face of the tool in the area close to the wear crater. As can be seen from the data presented, there is a high level of oxygen on the surface of the adherents of the machined material (in terms of the comparison of the areas of distribution of Fe and oxygen). Signs of oxidation are also visible on the unworn coating surface close to the wear crater (this can be seen from the comparison of the areas of distribution of oxygen and the main elements of the coatings). The presence of oxygen on the worn coating surface is insignificant, and its distribution is discrete, which can be mainly associated with the oxidation of the particles of the machined material (since the iron and oxygen locations coincide). Thus, it can be assumed that in this case, the coating surface adjacent to the cutting zone is exposed to oxidation. However, the presence of oxidized coating elements directly in the cutting zone is insignificant, which may be associated with the limited access of oxygen to the cutting zone because of the tight plastic contact between the cut-off material layer and the coating surface or the removal of the formed oxide particles by descending chips. It is possible that the factors described above have a simultaneous effect on the cutting tool (oxides are formed in small amounts and are quickly removed with the flow of the cut-off material).

3.4. Study of wear patterns on the coatings at v_c = 400 m/min

H1. Zr,Hf-(Zr,Hf)N-(Zr,Mo,Hf,Al)N

The area of the coating directly adjacent to the wear crater, but not a zone of dense plastic contact (secondary deformation zone) [81,82] with the flow of the cut-off material, was considered (Fig. 8). Fig. 8 exhibits that the coating surface bears a layer that is light in contrast, which was formed, presumably, as a result of oxidation. Areas A-E in this layer were chosen for the further research (Fig. 8).

The analysis of the oxide layer at the outer coating boundary (Fig. 9) suggests that this layer contains aluminum oxide, as well as iron oxide. It can be assumed that the oxide of aluminum in this layer has amorphous structure and its matrix contains crystalline particles of iron oxide [83]. The presence of zirconium and hafnium oxides is also possible. The studies revealed that this layer had noticeable differences in the composition of oxides. In some areas (Points 1 in Areas A and D), aluminum oxide dominates, while some zones exhibit the high content of zirconium oxide (Points 1 and 2 in Areas B and C). The outer boundary of this layer includes fragments dominated by iron oxide and metallic iron (Point 1 in Area C and Points 1 and 2 in Area E). This area (the area of elastic contact of the chips and the rake face of the tool) exhibits the predomination of elastic deformations, and plastic deformations are localized in surface protrusions and setting points, that is, the phenomena typical for dry friction are observed [82]. This area combines high temperature and free access of oxygen, which results in the formation of an oxide layer 20–70 nm thick. This layer is formed by oxides of aluminum, zirconium, and hafnium. The outer surface of this layer also includes iron and iron oxide, which are the result of elastic contact with the flow of the cut-off metal (chips). The presence of molybdenum

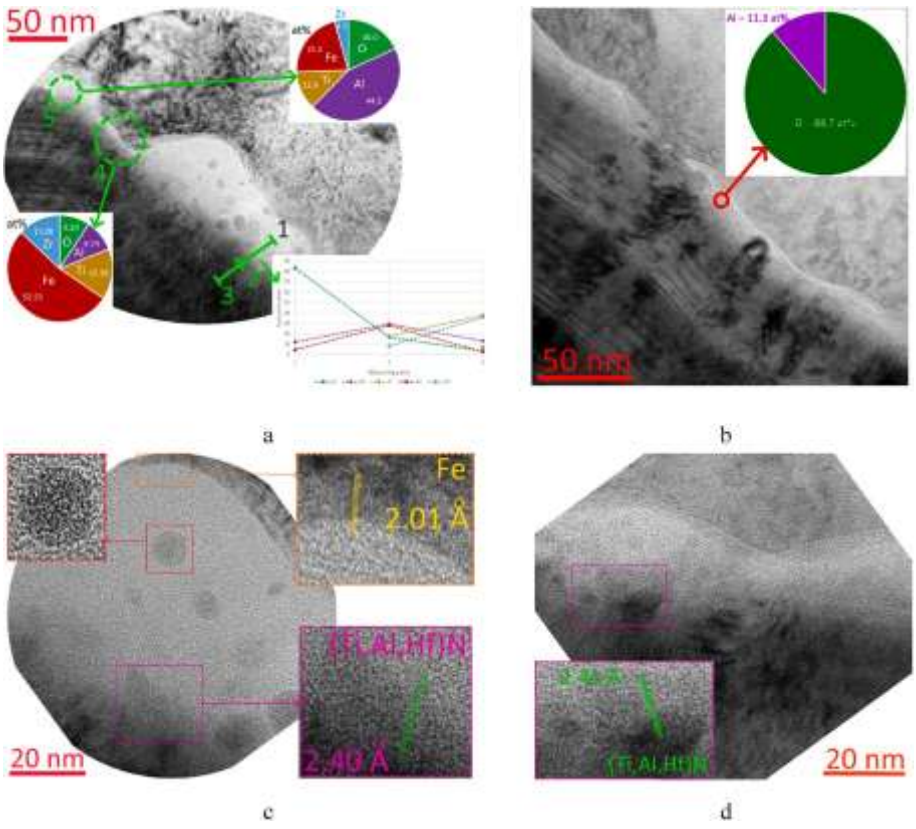

Fig. 13. (a,b) Analysis of the area of contact of the coating and the adherent of the machined material: the elemental analysis of the oxide layer, (c,d) the HRTEM analysis of the structure of the oxide layer.

oxides is possible (based on the distribution of elements), but they are not dominant in the studied areas.

The examination of the worn surface of this coating (Fig. 10) brings slightly different results. The worn surface of the coating bears a very thin oxide layer (25 nm thick). The small thickness of this layer makes it impossible to determine its exact phase composition with the available means. Based on the elemental composition, the presence of iron, zirconium, hafnium, or molybdenum oxides can be assumed. A noticeable aluminum content is observed at Point 2 (see the diagram in Fig. 10) and at Point 1 on the analysis line, which, being combined with the fairly high oxygen content, suggests the presence of aluminum oxide in these areas. No aluminum is detected at Points 1 and 3, which indicates the inhomogeneous composition of the layer under study. The SAED, obtained from the boundary of the worn area of the coating, depicts only reflections from the main cubic nitride phase of (Zr,Al,Hf)N. Iron diffuses into the coating to a depth of up to 300 nm. It should be noted that this area can be attributed rather to the region of elastic-plastic (a boundary of the region of purely plastic and purely elastic contacts), rather than plastic contact [82] due to the absence of any noticeable adherent of the machined material with clear signs of wear.

H2. Zr,Hf-(Zr,Hf)N-(Zr,Ti,Hf,Al)N

For Coating H2, like in the case of Coating H1, the coating area was chosen for the study as close as possible to the wear crater boundary and thus located in the area of elastic contact with the flow of the cut-off material [82] (Fig. 11 a). Like in Coating H1 considered earlier, the area under study bears an oxide surface layer that is light in contrast. The thickness of this layer is 20–50 nm (see Areas A-D in Fig. 11 b). The outer boundary of this oxide surface layer is dominated by metallic iron and iron oxide, while the inner layers can be assumed to contain oxides of titanium, zirconium, and hafnium (based on the ratio of oxygen and these elements). The high content of aluminum is detected in the central part of this layer (significantly higher than in the coating as a whole). The analysis of the change in the aluminum and oxygen content suggests the formation of aluminum oxide in this area. Thus, the formation of the oxide layer can be assumed to take place with the dominance of iron and iron oxide in the outer part, the high content of aluminum oxide in the central part, and the dominance of zirconium and titanium oxides in the inner region. A similar structure of the oxide layer is also observed in the region of Coating H1, which is similar in location.

Examination of the adherent-free surface of the worn coating (Fig. 12 a) reveals the presence of an area that may be an oxidized layer. However, the SAED analysis of this area did not find the phases other than the initial fcc phases of the coating. Although the study of the elemental composition reveals the diffusion of oxygen to a depth of up to 400 nm (Fig. 12 c), the oxygen content at such depths is quite low (about 2 at%). Thus, it is not possible to assume an oxide layer formed over the entire depth of oxygen diffusion. A sufficiently high concentration of oxygen, which allows assuming the presence of an oxide layer, is detected only in a region that is bright in contrast on the coating surface with the thickness of about 20 nm. Iron also diffuses into the coating to a depth of up to 500 nm. The study of the area of dense plastic contact (Fig. 12 b) detects the presence of an adherent, which contains iron and iron oxides. The layered structure of the adherent can be associated with different speeds of movement of the layers of the cut-off material, which occurs due to the deceleration of the inner layers during adhesive interaction with the coating surface. The SAED analysis also detected no oxide phases in this area. The elemental composition analysis (Fig. 12 d) suggests the presence of a very thin (no more than 10 nm thick) oxide layer. The obtained data can hardly contribute to a conclusion about the composition of this layer due to its small thickness. This layer most likely contains aluminum and zirconium oxides (the content of these elements slightly increases in this region). Oxides of iron are also likely to be present in this layer.

The examination of the area of dense plastic contact using HR TEM

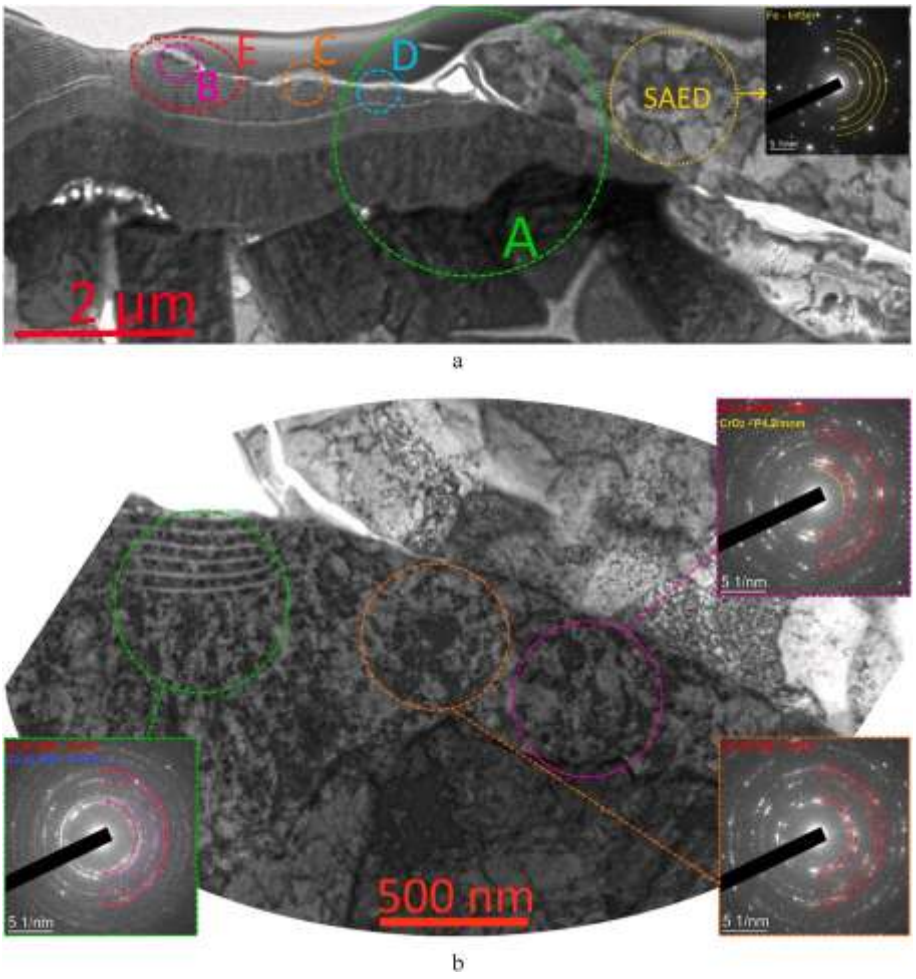

Fig. 14. (a) Overall view of the region under study of Coating H3 and localization of the considered areas A-F, (b) outcome of the SAED analysis of the area of contact between the adherent formed by the machined material and the coating.

(Fig. 13) contributed to the study in more detail of the oxide layer at the boundary of the coating and the adherent. Due to the high aluminum and oxygen content, the presence of aluminum oxide in this layer can be assumed with a high degree of certainty. The HREM study confirms that the layer of aluminum oxide has an amorphous structure, uniform in contrast, with spherical particles that stand out in the dark contrast. No reliable SAED result could be obtained because of the small width of this oxide layer. The analysis of interplanar spacings (Fig. 13 c and 13 d) detects the presence of metallic iron (d = 2.01 Å) and grains of (Ti,Al,Hf)N, one of the initial phases of the coating. Based on the analysis of the elemental composition of this region, it can be assumed that the amorphous structure, which is light in contrast, is an oxide of aluminum.

H3. Zr,Hf-(Zr,Hf)N-(Zr,Cr,Hf,Al)N

A region of transition from plastic to elastic contact (the region of elastic-plastic contact) was chosen (Fig. 14 a) to study the processes of oxidation and diffusion in Coating H3. The right part of the region includes an adherent of the machined material. The SAED analysis of this adherent finds that it is predominantly composed of metallic iron. There is a small amount of CrO_2 chromium oxide at the boundary of the coating and the adherent (Fig. 14 b). The SAED analysis of other zones at the coating boundary detects only initial fcc phases of the coating itself.

The elemental analysis of the area of contact between the coating and the adherent formed by the machined material (Fig. 15 a-c) did not detect a continuous layer of oxide on the coating surface. The adherent-free part of the coating surface (elastic contact area) can contain a slight oxide layer (Point 6 on Line L1 Fig. 15 a). The formation of iron oxides takes place in the adherent at the boundary with the coating. Fig. 15 b depicts the layered structure of the adherent: the oxidized layer (Points 1 and 2) and the metallic iron layer (Point 3). The adherent-free worn surface of the coating (supposed area of elastic-plastic contact) can be assumed to contain a layer of zirconium oxide with the thickness of up to 30 nm (Fig. 15 d).

Of particular interest is the pattern of wear of the coating nanolayers under the influence of the flow of the cut-off material in the case when the nanolayers are located at an acute angle to this flow. As can be seen from Fig. 16 a and 16 b, there is an "erosion" of the coating layer under the influence of a moving highly ductile metal layer. Such wear pattern can be a result of a combination of the adhesive-fatigue and diffusion processes.

The HRTEM analysis focused on the structure of the boundary of the coating and the adherent formed by the machined material (Fig. 16 c) revealed only a phase of iron oxide, while the SAED analysis also detected the presence of CrO_2 (see above). It has been found that oxides of the coating elements are not observed in the area, which indicates the absence of a continuous layer of oxide and the presence of these oxides only in the form of individual particles.

4. Conclusions

- The maximum microhardness is typical for Coating H2, and the minimum microhardness – for Coating H3. At temperatures up to 700 °C, the lowest value of the adhesive component f_{adh} of the friction coefficient was exhibited by Coating H3, and at temperatures

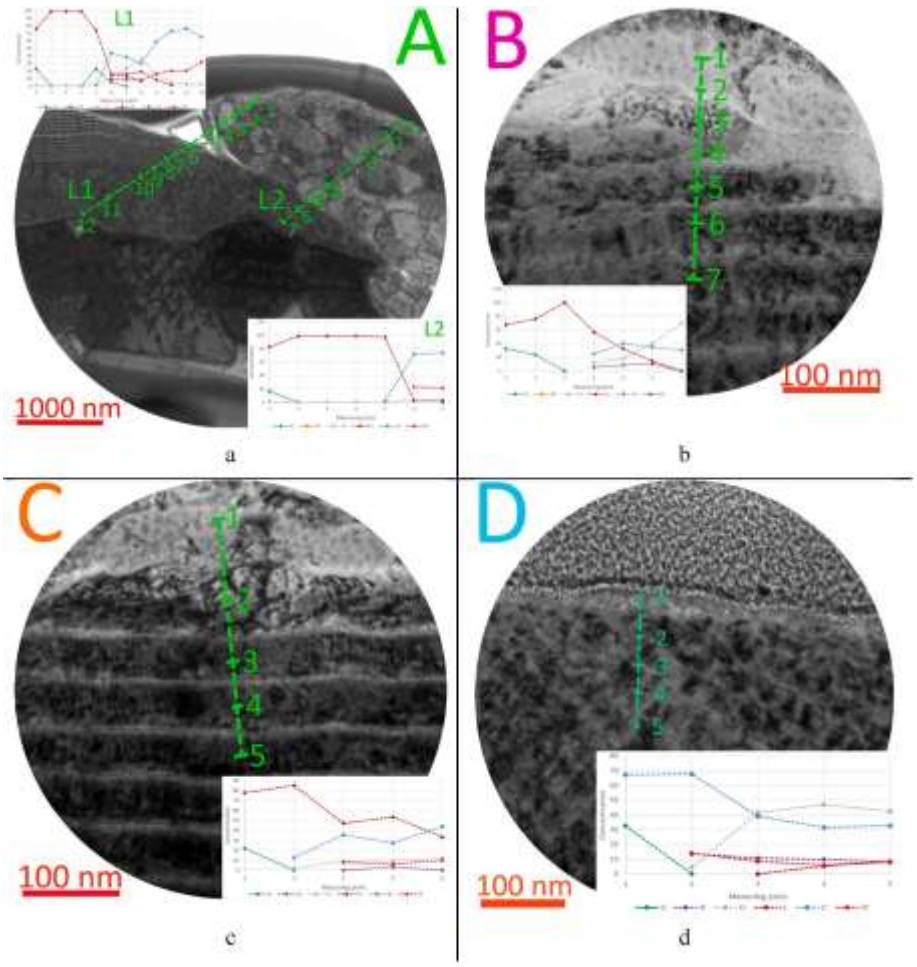

Fig. 15. Results of the studies of the processes of diffusion and oxidation in Coating H3: (a–c) the boundary of the coating and adherent formed by the machined material (Areas A-C, see location in Fig. 14 a), (d) worn area of the coating without adherent (Area D, see location in Fig. 14 a).

above 700 °C – by Coating H1. The best wear resistance in turning of steel at the speed of cutting $v_c = 250$ m/min was demonstrated by the tool with Coating H3, and at the speed of cutting $v_c = 400$ m/min – by the tool with Coating H1. Thus, the optimum coating composition depends on the speed of cutting.

- Information about the adhesive component f_{adh} of the friction coefficient makes it possible to predict the tool wear intensity quite well during the cutting under conditions of exposure to the temperatures corresponding to the temperatures at which the value of f_{adh} was measured.
- The studies of the wear patterns of the coatings at high speeds of cutting ($v_c = 400$ m/min) found that:
- in the coating areas adjacent to the wear crater (supposed area of elastic contact), an oxide layer up to 70 nm thick is formed. The elemental analysis of this layer revealed that:
  - the outer region of the layer is saturated with iron and iron oxide,
  - the intermediate region has a high content of aluminum oxide,
  - the area adjacent to the non-oxidized coating layers has a dominant content of zirconium, titanium, chromium, and hafnium oxides;
- the worn areas of the coating free of an adherent of the machined material (supposed region of elastic-plastic contact) include the oxide layer 20–25 nm thick, in which the presence of iron oxides and oxides of coating elements is assumed;
- no continuous oxide layer is observed in the region of plastic contact, but individual oxide particles, in particular, chromium oxide and zirconium oxide, may present;
- quite active formation of oxide films of coating elements is observed in the area close to the zone of cutting. At the same time, only minor oxide particles are detected directly in the wear area of the coating, and they can hardly have a significant effect on the process of cutting.
- in oxide-containing layers, an increased (relative to the initial) content of zirconium and a reduced content of hafnium are observed. This result can be interpreted as confirmation of the greater propensity of zirconium to oxidize, which was previously predicted based on a comparison of Gibbs free energy values.
- since the density of oxides is noticeably lower than the density of the corresponding nitrides (see Table 1), one can predict a significantly lower wear resistance of oxides formed on the surface of the coating.

Thus, it can be assumed that the formed oxide grains are destroyed rather quickly under the influence of the flow of the cut material, without having time to form a continuous oxide film in this area. Based on the foregoing, it can be concluded that under these cutting conditions, active oxide formation reduces the wear resistance of the coating (and, accordingly, the wear resistance of the tool). No positive effect of oxides on the wear resistance of the coating has been established; accordingly, the best wear resistance will be inherent in coatings that have the least tendency to oxide formation at high temperatures. The H3 coating (including chromium) showed the highest tendency to oxidize and the least wear resistance.

The H1 coating (with molybdenum) showed the best wear resistance (at $v_c = 400$ m/min) with a low tendency to oxidize. Further studies are

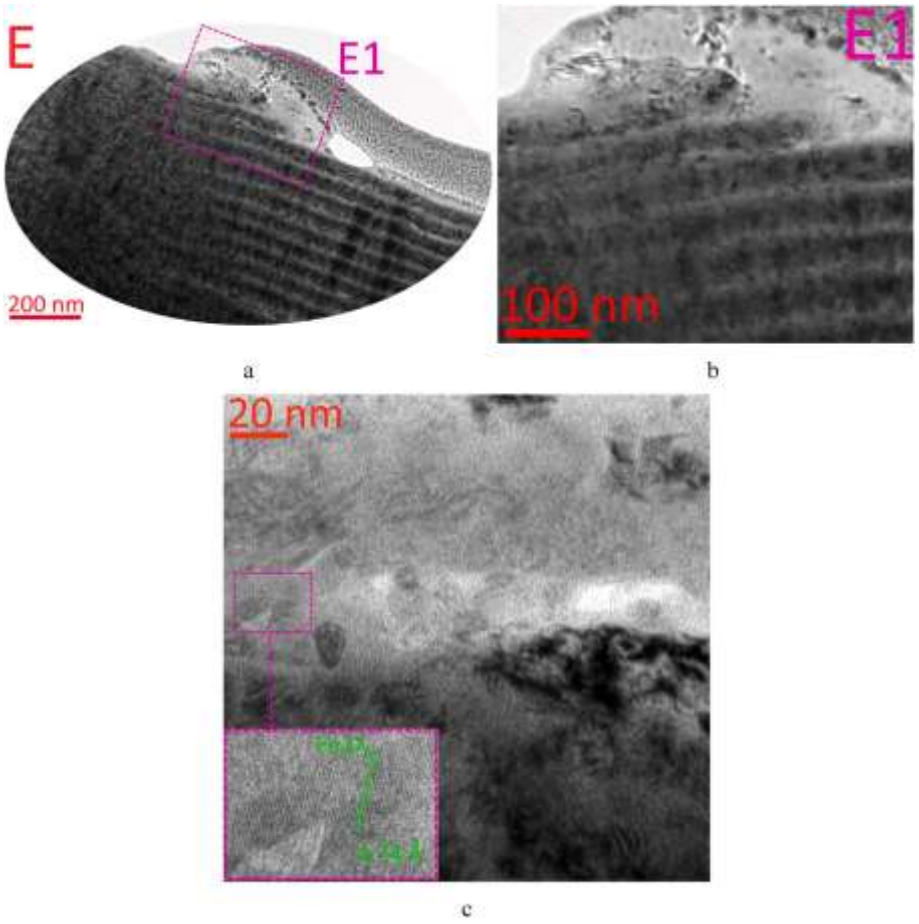

Fig. 16. (a,b) Wear pattern of the nanolayered structure of Coating H3 under the influence of the flow of the cut-off material, (c) results of the HRTEM analysis of the structure of the interface of the coating and the adherent formed by the machined material (Area E, see location in Fig. 14 a).

expected to consider a Zr,Hf-(Zr,Hf)N-(Zr,Hf,Mo,Al)N coating with a lower zirconium content or without zirconium. Presumably, reducing the zirconium content should increase the oxidation resistance.

Funding

The study was supported by a grant from the Russian Science Foundation (project No. 21-79-30058).

Acknowledgments

Authors conducted the studies using the equipment of the Center of collective use of MSTU "STANKIN" (agreement No. 075-15-2021-695, 26/07/2021). The structure of the coating was studied with the equipment of the Centre for collective use of scientific equipment "Material Science and Metallurgy", purchased with the financial support of the Ministry of Science and Higher Education of the Russian Federation (GK 075-15-2021-696).

References

[1] Z. Peng, H. Miao, L. Qi, S. Yang, C. Liu, Hard and wear-resistant titanium nitride coatings for cemented carbide cutting tools by pulsed high energy density plasma, Acta Mater. 51 (11) (2003) 3085–3094.

[2] J. Zhao, Z. Liu, B. Wang, J. Hu, Y. Wan, Tool coating effects on cutting temperature during metal cutting processes: comprehensive review and future research directions, Mech. Syst. Signal Process. 150 (2021), 107302.

[3] M. Kathrein, C. Michotte, M. Penoy, P. Polcik, C. Mitterer, Multifunctional multi-component PVD coatings for cutting tools, Surf. Coating. Technol. 200 (5–6) (2005) 1867–1871.

[4] K.D. Bouzakis, N. Michailidis, G. Skordaris, E. Bouzakis, D. Biermann, R. M'Saoubi, Cutting with coated tools: coating technologies, characterization methods and performance optimization, CIRP Ann. - Manuf. Technol. 61 (2012) 703–723.

[5] M. Tkadletz, N. Schalk, R. Daniel, J. Keckes, C. Czettl, C. Mitterer, Advanced characterization methods for wear resistant hard coatings: a review on recent progress, Surf. Coating. Technol. 285 (2016) 31–46.

[6] S. Zhang, D. Sun, F. Yongqing, D. Hejun, Recent advances of superhard nanocomposite coatings: a review, Surf. Coating. Technol. 167 (2003) 113–119.

[7] A. Vereschaka, V. Tabakov, S. Grigoriev, N. Sitnikov, N. Andreev, F. Milovich, Investigation of wear and diffusion processes on rake faces of carbide inserts with Ti-TiN-(Ti,Al,Si)N composite nanostructured coating, Wear 416–417 (2018) 72–80.

[8] K. Bobzin, High-performance coatings for cutting tools, CIRP J. Manufact. Sci. Technol. 18 (2017) 1–9.

[9] A.A. Vereschaka, M.A. Volosova, S.N. Grigoriev, A.S. Vereschaka, Development of wear-resistant complex for high-speed steel tool when using process of combined cathodic vacuum arc deposition, Procedia CIRP 9 (2013) 8–12.

[10] V.M. Beresnev, I.N. Torianyk, A.D. Pogrebnjak, O.V. Bondar, M. Bilokur, O. V. Sobol, D.A. Kolesnikov, S.V. Lytovchenko, P.V. Turbin, Structure and physical and mechanical Properties of nanocomposite (Zr-Ti-Cr-Nb)N and (Ti-Zr-Al-Nb-Y)N coatings, obtained by vacuum-arc evaporation method, Springer Proc. Phys. 156 (2015) 75–84.

[11] S.C. Liang, Z.C. Chang, D.C. Tsai, Y.C. Lin, H.S. Sung, M.J. Deng, F.S. Shieu, Effects of substrate temperature on the structure and mechanical properties of (TiVCrZrHf) N coatings, Appl. Surf. Sci. 257 (2011) 7709–7713.

[12] C.H. Lai, S.J. Lin, J.W. Yeh, S.Y. Chang, Preparation and characterization of AlCrTaTiZr multi-element nitride coatings, Surf. Coating. Technol. 201 (2006) 3275–3280.

[13] K.-S. Chang, K.-T. Chen, C.-Y. Hsu, P.-D. Hong, Growth (AlCrNbSiTiV)N thin films on the interrupted turning and properties using DCMS and HIPIMSsystem, Appl. Surf. Sci. 440 (2018) 1–7.

[14] S. PalDey, S.C. Deevi, Properties of single layer and gradient (Ti,Al)N coatings, Mater. Sci. Eng. 361 (1–2) (2003) 1–8.

[15] H. Klostermann, H. Fietzke, T. Modes, O. Zywitzki, Zr-Al-N nanocomposite coatings deposited by pulse magnetron sputtering, Rev. Adv. Mater. Sci. 15 (1) (2007) 33–37.

[16] P.H. Mayrhofer, H. Willmann, A.E. Reiter, Structure and phase evolution of Cr-Al-N coatings during annealing, Surf. Coating. Technol. 202 (20) (2008) 4935–4938.

[17] J.-K. Park, H.-J. Park, J.-H. Ahn, Y.-J. Baik, Effect of Ti to Al ratio on the crystalline structure and hardening of a $Ti_{1-x}Al_xN$/CrN nanoscale multilayered coating, Surf. Coating. Technol. 203 (20–21) (2009) 3099–3103.

[18] N.J.M. Carvalho, E. Zoestbergen, B.J. Kooi, J.ThM. De Hosson, Stress analysis and microstructure of PVD monolayer TiN and multilayer TiN/(Ti,Al)N coatings, Thin Solid Films 429 (1–2) (2003) 179–189.

[19] B.D. Beake, G.S. Fox-Rabinovich, Progress in high temperature nanomechanical testing of coatings for optimising their performance in high speed machining, Surf. Coating. Technol. 255 (2014) 102–111.

[20] G.S. Fox-Rabinovich, G.E. Totten, Self-Organization during Friction: Advanced Surface-Engineered Materials and Systems Design, Taylor & Francis Group LLC, Abingdon, UK, 2006, p. 461.

[21] R.A. Koshy, M.E. Graham, L.D. Marks, Temperature activated self-lubrication in CrN/Mo_2N nanolayer coatings, Surf. Coating. Technol. 204 (2010) 1359–1365.

[22] S.A. Glatz, V. Moraes, C.M. Koller, H. Riedl, H. Bolvardi, S. Kolozsv´ari, P. H. Mayrhofer, Effect of Mo on the thermal stability, oxidation resistance, and tribo-mechanical properties of arc evaporated Ti-Al-N coatings, J. Vac. Sci. Technol., A 35 (2017), 061515.

[23] H. Ju, D. Yu, J. Xu, L. Yu, B. Zuo, Y. Geng, T. Huang, L. Shao, L. Ren, C. Du, H. Zhang, H. Mao, Crystal structure and tribological properties of Zr-Al-Mo-N composite films, Mater. Chem. Phys. 230 (2019) 347–354.

[24] T. Suszko, W. Gulbin´ski, J. Jagielski, The role of surface oxidation in friction processes on molybdenum nitride thin films, Surf. Coating. Technol. 194 (2–3) (2005) 319–324.

[25] R. Pietruszka, B.S. Witkowski, S. Zimowski, T. Stapinski, M. Godlewski, Tribological study of hafnium dioxide and aluminium oxide films grown by atomic layer deposition on glass substrate, Thin Solid Films 709 (2020), 138191.

[26] S. Grigoriev, A. Vereschaka, F. Milovich, V. Tabakov, N. Sitnikov, N. Andreev, T. Sviridova, J. Bublikov, Investigation of multicomponent nanolayer coatings based on nitrides of Cr, Mo, Zr, Nb, and Al, Surf. Coating. Technol. 401 (2020), 126258.

[27] A.A. Vereschaka, S.N. Grigoriev, N.N. Sitnikov, A.D. Batako, Delamination and longitudinal cracking in multi-layered composite nano-structured coatings and their influence on cutting tool life, Wear 390–391 (2017) 209–219.

[28] M.H. Attia, A. de Pannemaecker, G. Williams, Effect of temperature on tribo-oxide formation and the fretting wear and friction behavior of zirconium and nickel-based alloys, Wear 476 (2021), 203722.

[29] A.N. Zelikman, B.G. Korshunov, Metallurgy of rare metals, Metallurgy, Moscow (1991) 430–p.

[30] X.J. Chen, V.V. Struzhkin, Z.G. Wu, M. Somayazulu, J. Qian, S. Kung, A. N. Christensen, Y.S. Zhao, R.E. Cohen, H.K. Mao, R.J. Hemley, Hard superconducting nitrides, Proc. Natl. Acad. Sci. USA 102 (2005) 3198–3201.

[31] A. Wang, S. Shang, D. Zhao, J. Wang, L. Chen, Y. Du, Z.-K. Liu, T. Xu, S. Wang, Structural, phonon and thermodynamic properties of fcc-based metal nitrides from first-principles calculations, Calphad Comput. Coupling Phase Diagrams Thermochem. 37 (2012) 126–131.

[32] M.A. Caravaca, J.C. Mīo, V.J. P´erez, R.A. Casali, C.A. Ponce, Ab initio study of the elastic properties of single and polycrystal TiO_2, ZrO_2 and HfO_2 in the cotunnite structure, J. Phys. Condens. Matter 21 (1) (2009), 015501.

[33] M. Ismail, M.K. Rahmani, S.A. Khan, J. Choi, F. Hussain, Z. Batool, A.M. Rana, J. Lee, H. Cho, S. Kim, Effects of Gibbs free energy difference and oxygen vacancies distribution in a bilayer ZnO/ZrO_2 structure for applications to bipolar resistive switching, Appl. Surf. Sci. 498 (2019), 143833.

[34] E.N. Kablov, V.L. Stolyarova, V.A. Vorozhtcov, S.I. Lopatin, F.N. Karachevtsev, Vaporization and thermodynamics of ceramics in the Y_2O_3-ZrO_2-HfO_2 system, Rapid Commun. Mass Spectrom. 33 (19) (2019) 1537–1546.

[35] E. Atar, E.S. Kayali, H. Cimenoglu, Sliding wear behaviour of ZrN and (Zr, 12 wt% Hf)N coatings, Tribol. Int. 39 (4) (2006) 297–302.

[36] D.A.R. Fernandez, B.S.S. Brito, I.A.D. Santos, V.F.D. Soares, A.R. Terto, G.B. de Oliveira, R. Hubler, W.W. Batista, E.K. Tentardini, Effect of hafnium contaminant present in zirconium targets on sputter deposited ZrN thin films, Nucl. Instrum. Methods Phys. Res. Sect. B Beam Interact. Mater. Atoms 462 (2020) 90–94.

[37] R. Kakanakov, Hr Bahchedjiev, L. Kolaklieva, T. Cholakova, Sv Evtimova, E. Polyhroniadis, E. Pavlidou, I. Tsiaoussis, Investigation of ZrN hard coatings obtained by cathodic arc evaporation, Solid State Phenom. 159 (2010) 113–116.

[38] T. Kuznetsova, V. Lapitskaya, B. Warcholinski, A. Gilewicz, S. Chizhik, Friction and wear of ZrN coatings under conditions of microcontact using atomic-force microscopy, J. Frict. Wear 41 (4) (2020) 287–294.

[39] E. Atar, H. Cimenoglu, E.S. Kayali, An investigation of fretting wear behaviour of a ternary (Zr,Hf)N coating, Proceedings of the World Tribology Congress III – (2005) 395–396.

[40] E. Atar, E.S. Kayali, H. Cimenoglu, Reciprocating wear behaviour of (Zr,Hf)N coatings, Wear 257 (5–6) (2004) 633–639.

[41] Z.T. Wu, Z.B. Qi, D.F. Zhang, Z.C. Wang, Microstructure, mechanical properties and oxidation resistance of (Zr, Hf)N_x coatings by magnetron co-sputtering, Surf. Coating. Technol. 276 (2015) 219–227.

[42] J. Prathumsit, G. Gitgeatpong, W. Phae-Ngam, C. Chananonnawathorn, T. Lertvanithphol, M. Horprathum, The effect of thickness on the properties of Zr-Hf-N thin films prepared by reactive co-magnetron sputtering, AIP Conf. Proc. 2279 (2020), 120004.

[43] C. Sarioglu, The effect of anisotropy on residual stress values and modification of Serruys approach to residual stress calculations for coatings such as TiN, ZrN and HfN, Surf. Coating. Technol. 201 (3–4) (2006) 707–717.

[44] E. Atar, C. Sarioglu, H. Cimenoglu, E.S. Kayali, Residual stresses in (Zr,Hf)N films (up to 11.9 at.% Hf) measured by X-ray diffraction using experimentally calculated XECs, Surf. Coating. Technol. 191 (2–3) (2005) 188–194.

[45] E. Atar, E.S. Kayali, H. Cimenoglu, The effect of oxidation on the structure and hardness of (Zr, Hf)N coatings, Defect Diffusion Forum 297–301 (2010) 1395–1399.

[46] C. Feng, S. Zhu, M. Li, L. Xin, F. Wang, Effects of incorporation of Si or Hf on the microstructure and mechanical properties of Ti-Al-N films prepared by arc ion plating (AIP), Surf. Coating. Technol. 202 (14) (2008) 3257–3262.

[47] Y.X. Xu, L. Chen, F. Pei, Y. Du, Y. Liu, J.L. Yue, Influence of Hf on the structure, thermal stability and oxidation resistance of Ti-Al-N coatings, Thin Solid Films 565 (2014) 25–31.

[48] R. Rachbauer, A. Blutmager, D. Holec, P.H. Mayrhofer, Effect of Hf on structure and age hardening of Ti-Al-N thin films, Surf. Coating. Technol. 206 (10) (2012) 2667–2672.

[49] F. Guo, D. Holec, J. Wang, S. Li, Y. Du, Impact of V, Hf and Si on oxidation processes in Ti–Al–N: insights from ab initio molecular dynamics, Surf. Coating. Technol. 381 (2012), 125125.

[50] E. Lugscheider, K. Bobzin, C. Pinero, F. Klocke, T. Massmann, Development of a superlattice (Ti,Hf,Cr)N coating for cold metal forming applications, Surf. Coating. Technol. 177–178 (2004) 616–622.

[51] K. Bobzin, N. Bagcivan, P. Immich, C. Warnke, F. Klocke, C. Zeppenfeld, P. Mattfeld, Advancement of a nanolaminated TiHfN/CrN PVD tool coating by a nano-structured CrN top layer in interaction with a biodegradable lubricant for green metal forming, Surf. Coating. Technol. 203 (20–21) (2009) 3184–3188.

[52] Z. Liu, H. Li, J. Li, J. Huang, J. Kong, D. Xiong, Tribological properties improvement of Mo-alloyed HfN films with a high H/E ratio at elevated temperatures, J. Tribol. 143 (1) (2021), 011704.

[53] U.S. Nyemchenko, V.M. Beresnev, V.F. Gorban, V.J. Novikov, O.V. Yaremenko, Comparing the tribological properties of the coatings (Ti-Hf-Zr-V-Nb-Ta)N and (Ti-Hf-Zr-V-Nb-Ta)N + DLC, J. Nano- and Electronic Physics 7 (3) (2015), 03041.

[54] F.F. Komarov, A.D. Pogrebnyak, S.V. Konstantinov, Physics of nanostructures at radiation resistance of high-entropy nanostructured (Ti,Hf,Zr,V,Nb)N coatings, Tech. Phys. 60 (10) (2015) 1519–1524.

[55] A.D. Pogrebnyak, V.M. Beresnev, D.A. Kolesnikov, M.V. Kaverin, A.P. Shypylenko, K. Oyoshi, Y. Takeda, R. Krause-Rehberg, A.G. Ponomarev, The effect of segregation and thermodiffusion on the formation of interfaces in nanostructured (Ti-Hf-Zr-V-Nb)N multielement coatings, Tech. Phys. Lett. 39 (3) (2013) 280–283.

[56] A.D. Pogrebnjak, V.N. Borisyuk, A.A. Bagdasaryan, O.V. Maksakova, E. V. Smirnova, The multifractal investigation of surface microgeometry of (Ti-Hf-Zr-V-Nb)N nitride coatings, J. Nano- and Electronic Physics 6 (4) (2014), 04018.

[57] U.S. Nemchenko, V.M. Beresnev, S.A. Klimenko, I.A. Podchernyaeva, P.V. Turbin, A.A. Andreev, Wear resistance of the multicomponent coatings of the (Ti-Zr-Hf-V-Nb-Ta)N system at elevated temperature, J. Superhard Mater. 37 (5) (2015) 322–326.

[58] K. Bobzin, High-performance coatings for cutting tools, CIRP J. Manufact. Sci. Technol. 18 (2017) 1–9.

[59] S.N. Grigoriev, M.A. Volosova, A.A. Vereschaka, N.N. Sitnikov, F. Milovich, J. I. Bublikov, S.V. Fyodorov, A.E. Seleznev, Properties of (Cr,Al,Si)N-(DLC-Si) composite coatings deposited on a cutting ceramic substrate, Ceram. Int. 46 (11) (2020) 18241–18255.

[60] A. Vereschaka, S. Grigoriev, V. Tabakov, M. Migranov Migranov, N. Sitnikov, F. Milovich, N. Andreev, Influence of the nanostructure of Ti-TiN-(Ti,Al,Cr)N multilayer composite coating on tribological properties and cutting tool life, Tribol. Int. 150 (2020), 106388.

[61] A. Vereschaka, V. Tabakov, S. Grigoriev, N. Sitnikov, F. Milovich, N. Andreev, C. Sotova, N. Kutina, Investigation of the influence of the thickness of nanolayers in wear-resistant layers of Ti-TiN-(Ti,Cr,Al)N coating on destruction in the cutting and wear of carbide cutting tools, Surf. Coating. Technol. 385 (2020), 125402.

[62] A.A. Vereschaka, J.I. Bublikov, N.N. Sitnikov, G.V. Oganyan, C.S. Sotova, Influence of nanolayer thickness on the performance properties of multilayer composite nano-structured modified coatings for metal-cutting tools, Int. J. Adv. Manuf. Technol. 95 (5–8) (2018) 2625–2640.

[63] S. Grigoriev, A. Vereschaka, V. Zelenkov, N. Sitnikov, J. Bublikov, F. Milovich, N. Andreev, C. Sotova, Investigation of the influence of the features of the

deposition process on the structural features of microparticles in PVD coatings, Vacuum 202 (2022), 111144.
[64] A.S. Vereschaka, A.A. Vereschaka, D.V. Sladkov, A.Y. Aksenenko, N.N. Sitnikov, Control of structure and properties of nanostructured multilayer composite coatings applied to cutting tools as a way to improve efficiency of technological cutting operations, J. Nano Res. 37 (2016) 51–57.
[65] S.N. Grigoriev, A.A. Vereschaka, S.V. Fyodorov, N.N. Sitnikov, A.D. Batako, Comparative analysis of cutting properties and nature of wear of carbide cutting tools with multi-layered nano-structured and gradient coatings produced by using of various deposition methods, Int. J. Adv. Manuf. Technol. 90 (9–12) (2017) 3421–3435.
[66] S. Grigoriev, M. Volosova, S. Fyodorov, M. Lyakhovetskiy, A. Seleznev, DLC-Coating application to improve the durability of ceramic tools, J. Mater. Eng. Perform. 28 (2019) 4415–4426.
[67] A. Vereschaka, V. Tabakov, S. Grigoriev, N. Sitnikov, F. Milovich, N. Andreev, J. Bublikov, Investigation of wear mechanisms for the rake face of a cutting tool with a multilayer composite nanostructured Cr–CrN-(Ti,Cr,Al,Si)N coating in high-speed steel turning, Wear 438–439 (2019), 203069.
[68] S.N. Grigoriev, M.A. Volosova, S.V. Fedorov, A.A. Okunkova, P.M. Pivkin, P. Y. Peretyagin, A. Ershov, Development of DLC-coated solid SiAlON/TiN ceramic end mills for nickel alloy machining: problems and prospects, Coatings 11 (5) (2021) 532.
[69] S. Grigoriev, A. Vereschaka, V. Zelenkov, N. Sitnikov, J. Bublikov, F. Milovich, N. Andreev, E. Mustafaev, Specific features of the structure and properties of arc-PVD coatings depending on the spatial arrangement of the sample in the chamber, Vacuum 200 (2022), 111047.
[70] C1624-05 Standard Test Method for Adhesion Strength and Mechanical Failure ASTM, Modes of Ceramic Coatings by Quantitative Single Point Scratch Testing, ASTM International, West Conshohocken, PA, USA, 2010.
[71] L.S. Shuster. Adhesive interaction of the cutting tool with the material being processed, Mashinostroenije, Moscow, 1988.
[72] S. Grigoriev, A. Vereschaka, F. Milovich, M. Migranov, N. Andreev, J. Bublikov, N. Sitnikov, G. Oganyan, Investigation of the tribological properties of Ti-TiN-(Ti, Al,Nb,Zr)N composite coating and its efficiency in increasing wear resistance of metal cutting tools, Tribol. Int. 164 (2021), 107236.
[73] A. Vereschaka, S. Grigoriev, F. Milovich, N. Sitnikov, M. Migranov, N. Andreev, J. Bublikov, C. Sotova, Investigation of tribological and functional properties of Cr, Mo-(Cr,Mo)N-(Cr,Mo,Al)N multilayer composite coating, Tribol. Int. 155 (2021), 106804.
[74] A.A. Vereschaka, S.N. Grigoriev, M.A. Volosova, A. Batako, A.S. Vereschaka, N. N. Sitnikov, A.E. Seleznev, Nano-scale multi-layered coatings for improved efficiency of ceramic cutting tools, Int. J. Adv. Manuf. Technol. 90 (1–4) (2017) 27–43.
[75] A.A. Vereschaka, A.S. Vereschaka, S.N. Grigoriev, A.K. Kirillov, O. Khaustova, Development and research of environmentally friendly dry technological machining system with compensation of physical function of cutting fluids, Procedia CIRP 7 (2013) 311–316.
[76] S.J. Suresha, R. Bhide, V. Jayaram, S.K. Biswas, Processing, microstructure and hardness of TiN/(Ti, Al)N multilayer coatings, Mater. Sci. Eng. 429 (1–2) (2006) 252–260.
[77] J.M. Longbottom, J.D. Lanham, A review of research related to Salomon's hypothesis on cutting speeds and temperatures, Int. J. Mach. Tool Manufact. 46 (14) (2006) 1740–1747.
[78] Z. P´almai, Proposal for a new theoretical model of the cutting tool's flank wear, Wear 303 (1–2) (2013) 437–445.
[79] X. Chuangwen, D. Jianming, C. Yuzhen, H. Li, S. Zhicheng, X. Jing, The relationships between cutting parameters, tool wear, cutting force and vibration, Adv. Mech. Eng. 10 (1) (2018).
[80] B. Wang, Z. Liu, Y. Cai, X. Luo, H. Ma, Q. Song, Z. Xiong, Advancements in material removal mechanism and surface integrity of high speed metal cutting: a review, Int. J. Mach. Tool Manufact. 166 (2021), 103744.
[81] N.A. Abukhshim, P.T. Mativenga, M.A. Sheikh, Heat generation and temperature prediction in metal cutting: a review and implications for high speed machining, Int. J. Mach. Tool Manufact. 46 (7–8) (2006) 782–800.
[82] M.F. Poletika, Contact Phenomena in Metal Cutting, Mashgiz. Moscow, 1963.
[83] S. Grigoriev, A. Vereschaka, F. Milovich, N. Andreev, J. Bublikov, N. Sitnikov, C. Sotova, N. Kutina, Investigation of wear mechanisms of multilayer nanostructured wear-resistant coatings during turning of steel. Part 2: diffusion, oxidation processes and cracking in Ti-TiN-(Ti,Cr,Mo,Al)N coating, 2021, Wear (2021) 486–487, 204096.